Journal of Multidisciplinary Healthcare

Dovepress
Taylor & Francis Group

Open Access Full Text Article

ORIGINAL RESEARCH

Deep Learning with Contrast-Enhanced Ultrasound for Preoperative Prediction of Early Recurrence in Hepatocellular Carcinoma After Hepatectomy

Dan Liu[1,*], Ke Yang[2,*], Chunquan Zhang[1,*], Zhen Hu[1], Yuan Cheng[1], Yunping Liu[1]

[1]Department of Ultrasound, The Second Affiliated Hospital, Jiangxi Medical College, Nanchang University, Nanchang, 330006, People's Republic of China; [2]The First In-Patient Department, Jiangxi Provincial People's Hospital, The First Affiliated Hospital of Nanchang Medical College, Nanchang, 330006, People's Republic of China

*These authors contributed equally to this work

Correspondence: Dan Liu, Department of Ultrasound, The Second Affiliated Hospital, Jiangxi Medical College, Nanchang University, No. 1, Minde Road, Donghu District, Nanchang, Jiangxi, 330006, People's Republic of China, Tel +86-15170076809, Email ultrald@163.com

Background: Hepatectomy is the primary curative treatment for early-stage hepatocellular carcinoma (HCC). However, postoperative early recurrence remains a significant challenge. The existing predictive approaches based on clinicopathological features lack sufficient accuracy. This study aimed to develop a deep learning (DL) framework using contrast-enhanced ultrasound (CEUS) to preoperatively predict early recurrence in patients with HCC undergoing hepatectomy.

Patients and Methods: In this retrospective study, a total of 115 patients with early-stage HCC who underwent preoperative CEUS were randomly divided into training (n=75) and validation (n=40) cohorts. Four DL models (CEUS-AP, CEUS-PP, CEUS-LP, and CEUS-MP) were developed using single-phase and multiphase CEUS cines. The CEUS-MP model, which integrated the arterial, portal venous, and late phases, was further combined with the clinical variables to construct a nomogram. Model performance was evaluated using the area under the receiver operating characteristic curve (AUC), sensitivity, and specificity.

Results: The CEUS-MP model demonstrated superior predictive performance, with AUCs of 0.922 and 0.840 in the training and validation cohorts, respectively, significantly outperforming single-phase models (all $P < 0.05$). The combined nomogram achieved AUCs of 0.945 and 0.871 in the training and validation cohorts, respectively, with a high sensitivity (88.9% and 83.0%, respectively) and specificity (98.1% and 82.5%, respectively). Decision curve analysis confirmed the nomogram's clinical utility for threshold probabilities >30%. Visualization maps highlighted heterogeneous enhancement patterns as the key predictive features.

Conclusion: The DL-based CEUS framework, particularly when integrated with clinical variables, provides a noninvasive and accurate tool for the preoperative prediction of early recurrence in patients with HCC undergoing hepatectomy.

Keywords: contrast-enhanced ultrasound, hepatocellular carcinoma, recurrence, deep learning

Introduction

Hepatocellular carcinoma (HCC) is one of the most prevalent and lethal malignancies worldwide, with hepatectomy remaining a primary curative treatment option for early-stage disease.[1,2] However, postoperative recurrence poses a significant challenge, with 5-year recurrence rate as high as 60%.[3] Recurrence can be categorized as early recurrence (<2 years), caused by micro metastases after resection, or late recurrence (>2 years), caused by new tumors arising in a microenvironment prone to carcinogenesis.[4] Research has shown that HCC patients who experience early recurrence post-resection have a worse prognosis compared to those with late recurrence.[5] Therefore, accurate prediction of early recurrence is critical for personalized postoperative surveillance and adjuvant therapy strategies.

Certain clinicopathological features, including the Barcelona Clinic Liver Cancer (BCLC) staging system, alpha-fetoprotein (AFP), microvascular invasion (MVI), and satellite nodules (SNs), have been linked to postoperative prognosis.[1,6] However, conventional predictive assessments based on these biomarkers lack sufficient predictive accuracy,

Received: 21 July 2025
Accepted: 15 October 2025
Published: 21 October 2025

and information on MVI and SNs is not available preoperatively. Several recent studies have used artificial intelligence models based on CT/MRI data to effectively predict the risk of postsurgical HCC recurrence risk.[7–10] Compared with CT and MRI, ultrasound possesses the advantages of real-time, radiation-free, and cost-effective, and can also be used for intraoperative evaluation and guide the operation pathway. Additionally, contrast-enhanced ultrasound (CEUS) has emerged as a valuable imaging modality for HCC, offering real-time dynamic assessment of tumor vascularity and perfusion characteristics.[11]

Previous studies have reported that certain CEUS characteristics such as rapid wash-in, early wash-out phase, rapid portal phase signal regression, and high LI-RADS grading are risk factors associated with early recurrence after radical HCC resection.[12,13] However, a critical gap remains: the interpretation of these characteristics is highly subjective and difficult to quantify, which limits their consistent application in prognostication. To address this gap in objectivity, deep learning (DL) emerges as a powerful tool. DL algorithms can automatically extract massive, quantitative features from medical images to model disease diagnosis and prognosis.[14] The application of DL to liver CEUS is already established for tasks such as focal liver lesion classification and predicting HCC biological behavior,[15,16] demonstrating its potential in this domain. However, these existing applications primarily focus on classification limited to single-phase analysis or static images, potentially overlooking the critical time-dependent kinetic information. The specific knowledge gap our study aims to fill is the use of DL to predict long-term clinical outcomes directly from pre-operative dynamic CEUS cines. Therefore, we hypothesize that a DL-based framework, by leveraging the rich temporal data in multiphase CEUS, can overcome the limitations of subjective interpretation. This study aims to develop and validate such a framework, integrating CEUS data with clinicopathological variables to provide a noninvasive and efficient preoperative tool for predicting early recurrence in patients with early-stage HCC after surgical resection.

Methods

Study Population and Design

This study was performed in accordance with the principles of the Declaration of Helsinki. This retrospective study was approved by the Ethics Committee of the Second Affiliated Hospital of Nanchang University (Approval No: IIT-O-2025-251). The requirement for informed consent was waived by the Ethics Committee due to the retrospective and minimal-risk nature of the study. All patient data were kept strictly confidential and de-identified prior to analysis. From January 2010 to January 2023, 155 patients with HCC who underwent CEUS within two weeks before hepatectomy were enrolled. The diagnosis of HCC was based on the diagnostic criteria established by the European Association for the Study of the Liver.[2] Inclusion criteria were: BCLC stage 0 or A; liver function with Child-Pugh class A or B; performance status Eastern Cooperative Oncology Group score 0 or 1; R0 resection;[17] regular follow-up within two years after hepatectomy. The exclusion criteria were poor CEUS imaging quality, recurrent HCC or primary HCC combined with other primary tumors, and a history of antitumor treatment before surgery, such as radiofrequency ablation, microwave ablation, transcatheter arterial chemoembolization, or chemotherapy. Pretreatment baseline clinical characteristics, including demographic data, laboratory test results, and clinical diagnoses, were collected from the Institutional Picture Archiving and Communication System (PACS®; Carestream Health, Toronto, Canada). Finally, 115 patients' preoperative CEUS cines and clinical variables were retrospectively analyzed. We developed four CEUS-based AI models to preoperatively predict early recurrence: CEUS-AP, CEUS-PP, CEUS-LP, and CEUS-MP. We further integrated clinical variables into the CEUS AI model to construct an individualized nomogram for preoperative prediction of early recurrence. The patient enrollment workflow and study design were shown in Figure 1.

CEUS Data Acquisition

CEUS was performed by one of two radiologists (ZH and YC) with over 10 years of experience in liver CEUS. Two types of ultrasound instruments were used in this study, Toshiba Aplio (n = 98) and SuperSonic Imagine (n = 17). The system parameters, including gain, dynamic range, mechanical index, output power, and focal zone, were fine-tuned to ensure effective tissue signal reduction without compromising penetration capability. A volume of 2.4 mL of the second-generation contrast agent (SonoVue®; Bracco Imaging, Milan, Italy) was injected within one second via the elbow,

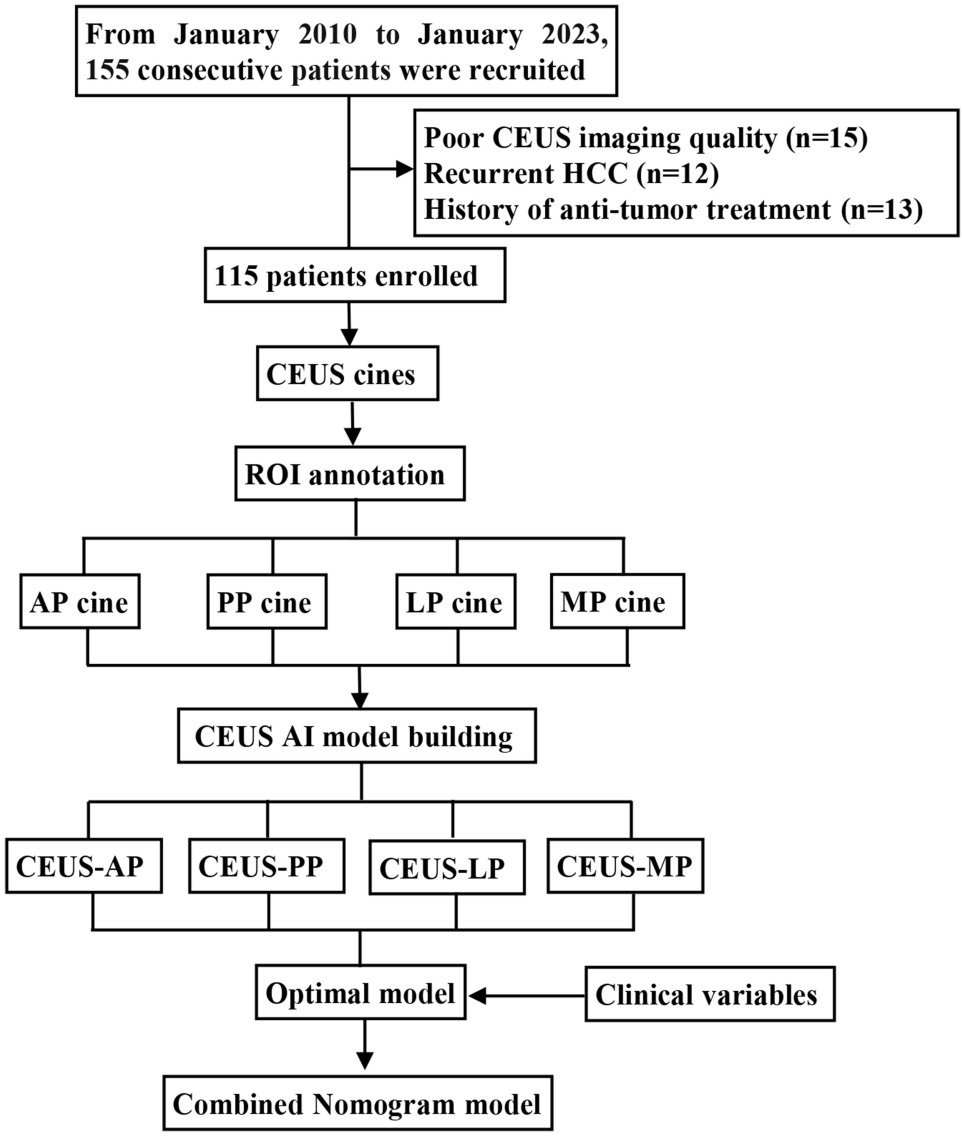

Figure 1 Study workflow flowchart.
Abbreviations: CEUS, contrast-enhanced ultrasound; HCC, hepatocellular carcinoma; ROI annotation illustration; AP, arterial phase; PP, portal venous phase; LP, late phase; MP, multiple phases.

followed by a 5-mL saline flush. The transducer was maintained in a stable position to continuously observe perfusion of the lesion. Three-phase contrast enhancement was dynamically monitored, consisting of arterial phase (AP, 0–30 s), portal venous phase (PP, 31–120 s), and late phase (LP, 121–360 s). The CEUS digital video recordings were stored as DICOM format.

Hepatectomy Procedure and Follow-Up Protocol

Anatomical partial hepatectomy was performed with a resection margin of ≥ 10 mm. All enrolled tumors were safely and completely removed, with no residual tumors following resection (R0 classification). The patients underwent regular follow-up assessments at 1, 3, 6, 9, and 12 months postoperatively, followed by evaluations every 3–6 months thereafter. During these visits, contrast-enhanced imaging (CEUS, CECT, or CEMRI) and serum biomarker testing (AFP and liver function) were performed. In this study, early recurrence was defined as a new lesion with typical imaging features of HCC that appeared in imaging examinations within 2 years after hepatectomy or as confirmed by pathological results from percutaneous liver biopsy or a second surgery.

Developing Prediction Model Based on CEUS

This study employed CEUS cines from three phases (arterial phase, portal venous phase, and late phase) to construct the corresponding single-phase models (CEUS-AP, CEUS-PP, and CEUS-LP). We then developed a comprehensive CEUS-MP (multi-phase) model that integrated all three phases. In each patient, three separate regions of interest (ROIs) were outlined by a radiologist with 5-year experience in CEUS to enable quantitative assessment of the CEUS videos across the arterial, portal venous, and late phases. The annotation tool was ITK-SNAP, which is an open-source software.[18] Specifically, the doctor first annotated the contour of the tumor in the CEUS frame when the tumor displayed clearly. A rectangle to cover the tumor contour and an approximately 0.5 cm wide liver parenchyma surrounding the tumor were created (Figure 2). All frames with the same ROI location determined in the annotated frame were cropped and manually adjusted if necessary. To assess inter-observer variability in ROI delineation, two doctors (one with more than 10 years of experience in CEUS and the other with more than 5 years of experience) independently contoured the ROIs for a randomly selected cohort of 30 patients, blinded to patient outcomes and clinical characteristics. Radiomic features extracted from both sets of ROIs were compared using the intraclass correlation coefficient (ICC) to determine feature reproducibility.

Enrolled patients were randomly divided into training (n = 75) and validation (n = 40) cohorts. To minimize model-induced bias, convolutional neural networks (CNN) were employed for the four models based on CEUS cines in different phases consisting of a two-dimensional (2D) convolution layer, 2D max-pooling layer, ReLU activation function, vector of locally aggregated descriptors (VLAD), and a fully connecting layer (FCL) (Figure 3). The inputs of the CEUS-AP, CEUS-PP, CEUS-LP, and CEUS-MP models were different CEUS cines in the arterial, portal venous, late, and the above-mentioned three phases, respectively. In the four CEUS AI models, convolution layers automatically learn the imaging features from each frame of CEUS, and VLAD is responsible for the quantitative analysis of enhancement patterns over time for the CEUS cines. The FCL guide model predicted the probability of early recurrence for each patient. A ten-fold validation method was adopted in the training phase to optimize the four CEUS AI models. To improve the prediction performance and reduce the risk of overfitting, CEUS cines were split over time into multiple independent samples at two frames per second; in this way, the training population was augmented for better learning. Data augmentation techniques, including random rotations, flips, and intensity variations, were employed to augment the diversity of the training dataset. Moreover, depth-wise convolution was selected to reduce the number of parameters in the training phase. Both L1 and L2 regularization were employed to combat overfitting. L1 regularization promoted sparsity and can perform feature selection by driving less important weights to zero, while L2 regularization penalized large weights to ensure the model was less sensitive to small fluctuations in the input data. This combined approach was chosen to create a more robust and generalizable model given the high-dimensional feature

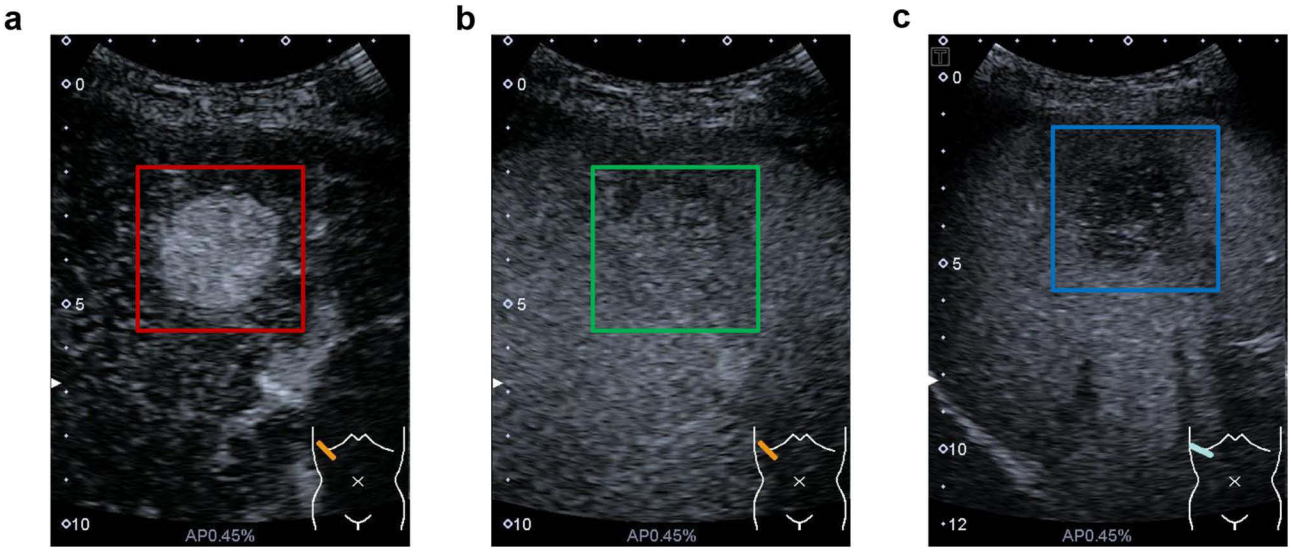

Figure 2 ROI annotation illustration. (**a**–**c**) An example of the red/green/blue rectangle ROI segmented in one AP/PP/LP CEUS frame when the tumor displayed clearly.
Abbreviations: ROI, region of interest; AP, arterial phase; PP, portal venous phase; LP, late phase; CEUS, contrast-enhanced ultrasound.

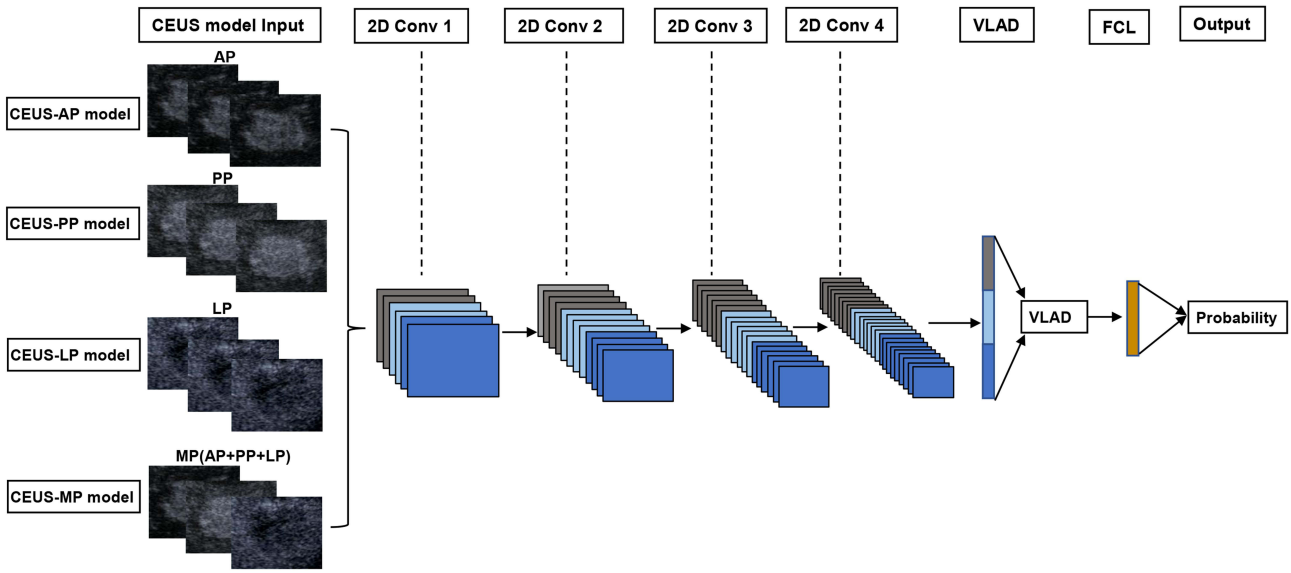

Figure 3 The overall network structure of CEUS AI models. CNN were employed for the four models based on CEUS cines in different phases. Input step: The CEUS cines of AP/ PP/LP/MP were inputted into the CNN model, respectively. Feature extraction step: The features extracted from three phases were then integrated into one feature collection which demonstrated the characteristics of the entire CEUS cine. 2D Conv x included 2D convolution layer, 2D max-pooling layer, and ReLU activation function. Output step: probability was calculated to estimate risk of early recurrence after hepatectomy.

Abbreviations: CEUS, contrast-enhanced ultrasound; AI, artificial intelligence; CNN, convolutional neural network; AP, arterial phase; PP, portal phase; LP, late phase; MP, multiple phases; 2D Conv, two-dimensional convolution; VLAD, vector of locally aggregated descriptors; FCL, full connected layer.

space relative to our sample size. We implemented early stopping based on the validation loss to halt training once performance on the validation set ceased to improve. In this study, the convolutional layers employed a depthwise separable convolution structure to replace the conventional 3D convolution operations, separating the processes of feature convolution filtering and the integration of cross-channel features. A global pooling layer was incorporated before the fully connected layers, aggregating features across temporal and spatial dimensions to reduce the number of neural nodes that the fully connected layers need to process. Through a series of specialized network design strategies, the parameter count of R-DLCEUS was reduced to approximately 20,000. During the training phase, the model used cross-entropy as the objective function and optimized the parameters using the stochastic gradient descent method. Each batch consisted of 16 samples, and the model was trained for 70 epochs. The initial learning rate was set to 0.001 and was reduced by a factor of 0.5 at the 15th, 30th, and 55th epochs. A momentum coefficient of 0.9 was applied during training. For the CEUS-MP model, the single-channel cine loops from the AP, PP, and VP were concatenated along the channel dimension to form a multi-channel input, which was then processed by the subsequent 2D convolutional network. The area under the receiver operating characteristic curve (AUC) was adopted to quantitatively measure the prediction performance of the CEUS AI models.

Building Combined Individualized Nomogram

To incorporate information from clinical variables with CEUS cines, an individualized model was developed to preoperatively predict early recurrence after hepatectomy. Specifically, four models developed from CEUS video data (CEUS-AP, CEUS-PP, CEUS-LP, and CEUS-MP) were evaluated to identify the optimal predictive model. Subsequently, the predictive probability of the selected model was used as a Radiomics signature and integrated with clinical variables to build a combined nomogram prediction model based on the multi-variable logistic regression analysis. In order to demonstrate the incremental value of DL-CEUS-based nomogram, univariate and multivariate logistic regression analyses were performed to build the Clinical-only model. The analyzed clinical variables included 16 basic clinical characteristics (Table 1). Variable selection followed a two-stage process. First, all parameters showing marginal significance ($P < 0.10$) in univariate analyses were included; subsequently, these were incorporated into a stepwise multivariable regression model. Only variables demonstrating statistical significance ($P < 0.05$) in the final multivariable

Table 1 Baseline Characteristics of Patients

Variables	All Patients (n=115)	Training Cohort (n = 75)	Validation Cohort (n = 40)	*P* value
Age (year)	55.41±14.62(29–79)	56.4±10.5(29–79)	54.1±11.5(32–68)	0.978
Sex (Male/Female)	93/22(80.9%/19.1%)	63/12(84.0%/16.0%)	30/10(75.0%/,25.0%)	0.261
Size, cm	3.1 (1.0–5.0)	2.9 ± 1.8	3.2 ± 1.6	0.504
Liver cirrhosis (Yes/No)	66/49(57.4%/42.6%)	41/34(54.7%/45.3%)	24/16(60.0%/40.0%)	0.584
ALT, U/L	47.7±36.1(4.8–224.0)	42.7±30.6(4.8–224.0)	45.8±37.2(11.0–194.0)	0.859
TBIL, μmol/L	17.2±10.2(4.0–72.2)	18.5±9.5(4.0–72.2)	18.9±10.4(5.6–67.9)	0.406
PT, s	13.2±1.7(10.9–23.2)	13.0±1.4(10.9–19.5)	13.1±1.7(10.9–23.2)	0.558
WBC, $\times 10^9$/L	5.9±4.1(1.2–46.0)	5.5±2.0(1.1–12.0)	6.3±5.3(2.3–46.0)	0.126
PLT, $\times 10^9$/L	152.9±77.4(17.0–468.0)	156.9±79.4(17.0–468.0)	148.6±64.0(61.0–324.0)	0.464
ALB, g/L				0.350
(< 35/≥ 35)	30/85(26.1%/73.9%)	17/58(22.7%/77.3%)	13/27(32.5%/67.5%)	
AFP, ng/mL				0.075
(<200/≥200)	84/31(73.0%/27.0%)	58/17(77.3%/22.7%)	26/14(65.0%/35.0%)	
Performance status				0.061
(0/1)	100/15(87.0%/13.0%)	62/13(82.7%/17.3%)	38/2(95.0%/5.0%)	
Tumor location				0.716
(Right lobe/Left lobe/Bilobar)	85/19/11(73.9%/16.5%/9.6%)	58/10/7(77.3%/13.3%/9.4%)	27/9/4(67.5%/22.5%/10.0%)	
Located in periphery of liver				0.671
(Yes/No)	47/68(40.9%/59.1%)	25/50(33.3%/66.7%)	22/18(55.0%/45.0%)	
Perivascular location				0.739
(Yes/No)	28/87(24.3%/75.7%)	16/59(21.3%/78.7%)	12/28(30.0%/70.0%)	
Early recurrence	30/115, 26.1%	18/75(24.0%)	12/40(30.0%)	NA

Abbreviations: ALT, alanine aminotransferase; TBIL, total bilirubin; PT, prothrombin time; WBC, white blood cell; PLT, platelet count; ALB, albumin; AFP, alpha-fetoprotein.

analysis were retained as independent predictors and were used for combined nomogram development. The prediction performance of the nomogram was assessed using AUC, calibration curves, and decision curves.

Visualization of the CEUS-MP Model

To enhance the interpretability of the DL model's predictions regarding early recurrence, we employed Selvaraju R.'s method to transform the DL feature maps into pseudo-colored visualization maps.[19] In these maps, warm-colored (red) pixels represent regions with stronger predictive relevance, indicating high-weight features that significantly contribute to the model's output. Conversely, the cool-colored (blue) pixels denote areas of weaker correlation corresponding to the low-weight factors in the prediction. This visualization approach effectively highlights the critical image regions that influence the model's decision-making process.

Statistical Analysis

The statistical software and packages used were Python (version 3.11), PyTorch (version 2.0.1), R (version 3.4.4), and computeC. The chi-square test was used to compare categorical variables. Student's *t*-test or the Mann–Whitney test, as appropriate, was used to compare continuous variables. All statistical tests were two-sided, and differences were considered significant at $P < 0.05$.

Results

Clinical Characteristics

Among 115 patients, there were 93 males (93/115, 80.9%) and 22 females (22/115, 19.1%). The mean tumor size was 3.1 ± 0.9 cm (range, 1.0–5.0 cm). Postoperative follow-up results revealed that among the115 patients, 30 (30/115, 26.1%) experienced early recurrence, whereas 85 (85/115, 73.9%) showed no evidence of early recurrence. There were no significant differences in the baseline characteristics between the training (n = 75) and validation (n = 40) cohorts. Detailed baseline characteristics of the two cohorts are shown in Table 1.

Predictive Performance of CEUS AI Models

The features demonstrated high reproducibility, with 91% achieving excellent ICC values, indicating strong inter-observer agreement in ROI segmentation. In the training cohort, AUCs of CEUS-MP, CEUS-AP, CEUS-PP, and CEUS-LP reached 0.922 (95% CI: 0.816–0.971), 0.829 (95% CI: 0.712–0.954), 0.816 (95% CI: 0.697–0.941) and 0.808 (95% CI: 0.691–0.938), respectively. The DL-based AI model using multiple CEUS cines (CEUS-MP) achieved the best prediction performance compared with the other three models based on single-phase CEUS cine (CEUS-AP, CEUS-PP, and CEUS-LP) (Figure 4a). Similar results were observed in the validation cohort. In the validation cohort, the AUCs of CEUS-MP, CEUS-AP, CEUS-PP, and CEUS-LP were 0.840 (95% CI: 0.701–0.989), 0.741 (95% CI: 0.670–0.921), 0.719 (95% CI: 0.637–0.909), and 0.703 (95% CI: 0.661–0.889), respectively (Figure 4b). Table 2 provides an overview of the quantitative assessment of the four models. CEUS-MP offered significantly higher AUCs than CEUS-AP, CEUS-PP, and CEUS-LP in both training ($P = 0.026$, $P = 0.014$, $P = 0.001$) and validation ($P = 0.029$, $P = 0.016$, $P = 0.001$) cohorts. However, no significant differences in AUCs were observed between CEUS-AP, CEUS-PP, and CEUS-LP in either the training or validation cohorts (all $P > 0.05$).

The Individualized Predictive Value of Combined Nomogram

Multivariable regression analysis revealed that serum albumin (< 35 g/L) (HR = 1.146, $P = 0.034$), AFP (> 1000 ng/mL) (HR = 1.908, $P = 0.028$), and the CEUS-MP signature (HR = 5.141, $P < 0.001$) were independent preoperative predictors of early recurrence (Table 3). An individualized nomogram was built based on these three significant values (Figure 5a). In the training and validation cohorts, the AUCs of the nomogram for early recurrence was 0.945 (95% CI: 0.861–0.965) and 0.871 (95% CI: 0.751–0.970) for early recurrence, respectively. (Figure 5b). The nomogram achieved a sensitivity of 88.9% (95% CI: 75.9–96.1%) and specificity of 98.1% (95% CI: 81.6–99.1%) in the training cohort. In the validation cohort, the sensitivity and specificity of the nomogram were 83.0% (95% CI: 70.4–90.8%) and 82.5% (95% CI: 70.8–91.5%), respectively. The nomogram showed good calibration for early recurrence prediction (Figure 5c). The Hosmer-Lemeshow test showed that there were no significant differences in early recurrence prediction between the nomogram and the ideal reference curve ($P = 0.415$). The decision curve analysis of the nomogram is presented in

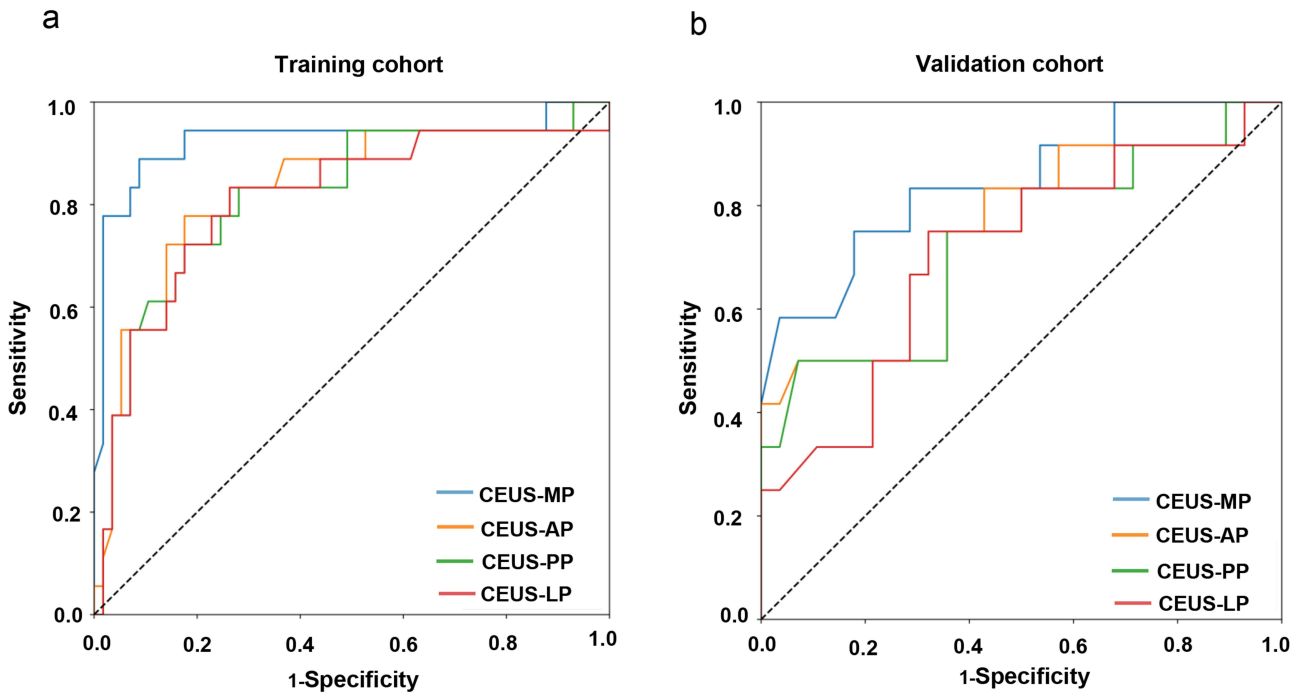

Figure 4 ROC curves of four CEUS AI models. (**a**) ROC curves of CEUS AI models in training cohort. (**b**) ROC curves of CEUS AI models in validation cohort. CEUS-MP achieved the best prediction performance compared with CEUS-AP, CEUS-PP, and CEUS-LP in both cohorts.

https://doi.org/10.2147/JMDH.S555110

Table 2 Predictive Performance of CEUS-MP, CEUS-AP, CEUS-PP, and CEUS-LP in Training and Validation Cohorts

Patient Number	AUC	Sensitivity, %	Specificity, %	Accuracy
CEUS-MP				
T 75(65.2%)	0.922(0.816–0.971)	88.9(70.1–97.2)	91.1(69.0–96.1)	0.930(0.909–0.989)
V 40(34.8%)	0.840(0.701–0.989)	78.2(69.0–86.1)	82.0(70.4–90.2)	0.819(0.780–0.943)
CEUS-AP				
T 75(65.2%)	0.829(0.712–0.954)	77.7(67.8–86.2)	81.3(74.1–90.5)	0.838(0.721–0.965)
V 40(34.8%)	0.741(0.670–0.921)	74.0(65.7–87.7)	72.5(66.8–85.3)	0.719(0.641–0.801)
CEUS-PP				
T 75(65.2%)	0.816(0.697–0.941)	80.1(74.2–87.6)	71.6(631–82.9)	0.818(0.712–0.976)
V 40(34.8%)	0.719(0.637–0.909)	71.5(66.8–88.5)	73.1(62.6–85.9)	0.710(0.681–0.832)
CEUS-LP				
T 75(65.2%)	0.808(0.691–0.938)	78.1(70.5–87.6)	76.8(67.2–85.1)	0.816(0.710–0.925)
V 40(34.8%)	0.703(0.661–0.889)	74.0(68.2–86.7)	67.8(62.4–78.3)	0.693(0.615–0.812)

Note: 95% confidence intervals for quantitative data are shown in brackets, when applicable.
Abbreviations: AUC, area under the receiver-operator-characteristic curve; T, training cohort; V, validation cohort; CEUS, contrast-enhanced ultrasound; AP, arterial phase; PP, portal venous phase; LP, late phase; AUC, area under the receiver operating characteristic curve.

Table 3 Prognostic Factors to Predict Early Recurrence of HCC Patients After Hepatectomy

Variables	Univariate	Multivariate	
	***P* value**	**HR (95% CI)**	***P* value**
CEUS-MP signatures	< 0.001	5.141(2.925–6.807)	< 0.001
Age	0.169		
Gender	0.510		
Liver cirrhosis	0.146		
ALT	0.109		
TBIL	0.386		
PT	0.238		
WBC	0.703		
PLT	0.862		
ALBI score	0.125		
ALB	0.032	1.146(0.260–2.294)	0.034
AFP	0.018	1.908(0.571–2.483)	0.028
Performance status	0.562		
Size	0.463		
Tumor location	0.194		
Perivascular location	0.214		
Located in periphery of liver	0.436		

Abbreviations: ALT, alanine aminotransferase; TBIL, total bilirubin; PT, prothrombin time; WBC, white blood cell; PLT, platelet count; ALBI scores, Albumin-Bilirubin scores; ALB, albumin; AFP, alpha-fetoprotein.

Figure 5d. AFP and serum albumin were selected to construct a Clinical-only model. The Clinical-only model had an AUC of 0.573 (95% CI: 0.501–0.675) in the training cohort with a 0.554 (95% CI: 0.512–0.685) accuracy and an AUC of 0.528 (95% CI: 0.500–0.618) in the validation cohort with a 0.545 (95% CI: 0.509–0.678) accuracy. The nomogram achieved a significantly higher predictive performance compared to the Clinical-only model in both training and validation cohorts (Both $P < 0.001$). The decision curves showed that if the threshold probability of a patient was > 30%, integrating CEUS-MP signatures and clinical variables (AFP and serum albumin) to predict the patient's early recurrence

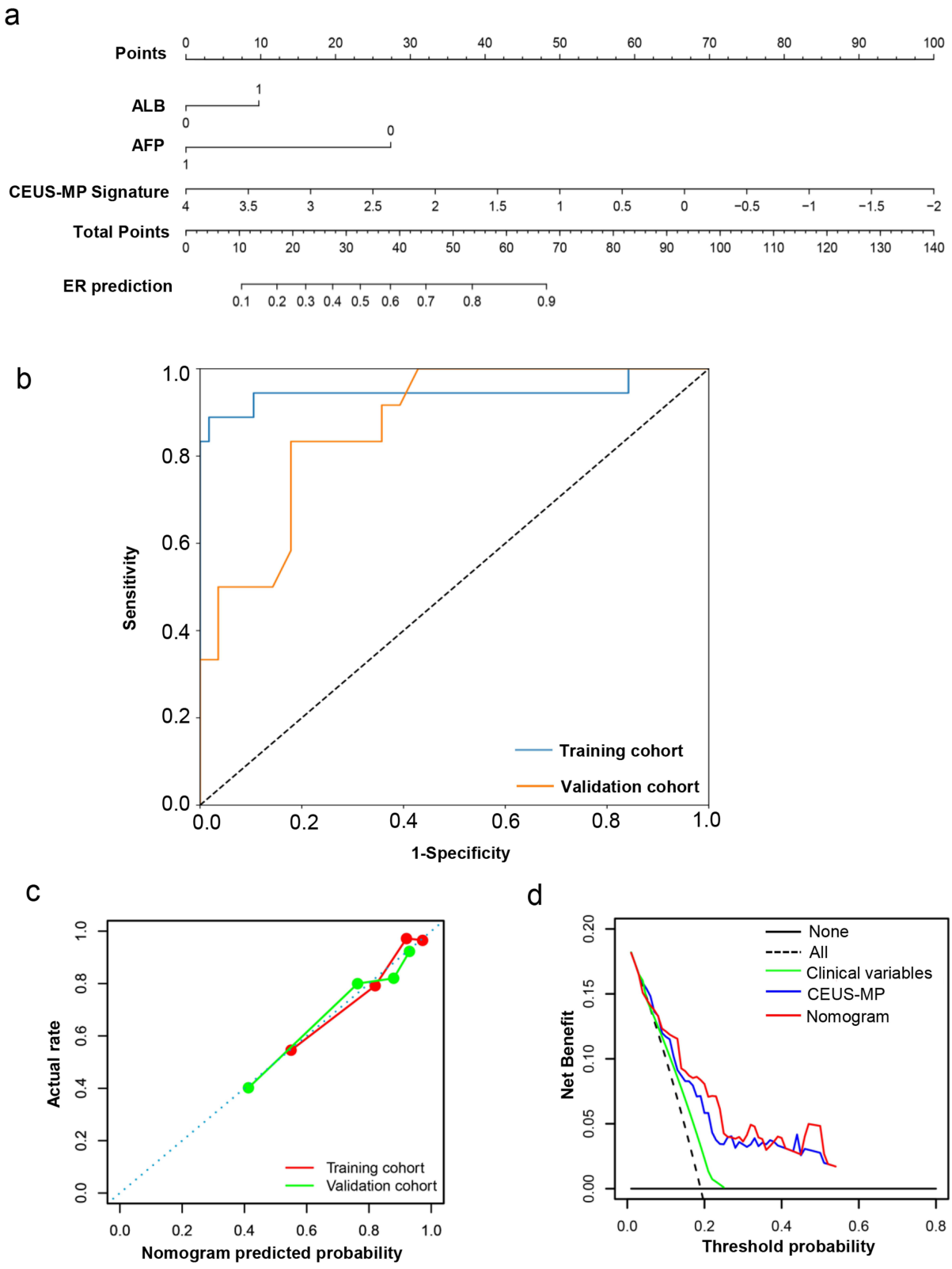

Figure 5 Prediction performance of individualized nomogram, ROC curves, calibration curves and Decision curve analysis. (**a**) Nomogram for predicting the probability of a patient occur early recurrence after hepatectomy. A patient who obtained high total scores of the three factors tends to have high probability of early recurrence after hepatectomy. ALB, 0 means < 35 g/L, 1 means ≥ 35 g/L; AFP, 0 means < 200ng/ mL, 1 means ≥ 200ng/mL. (**b**) ROC curves of nomogram in training and validation cohort. (**c**) Calibration curves of the nomogram for predicting early recurrence in training and validation cohorts. (**d**) Decision curve analysis for nomogram.

https://doi.org/10.2147/JMDH.S555110

added more net benefit than using only clinical variables. In addition, the net benefit of the CEUS-MP signature was similar to that of the nomograms.

Understanding the R-DLCEUS Model

From the visualization maps of the CEUS-LP model, it can be observed that the model focuses more on the early period AP, suggesting its potential ability to capture the "fast-in" feature, which may be closely associated with the early recurrence of HCC. Additionally, we observed that for some early cases, the attention of the model exhibited a "patchy" pattern (Figure 6). We

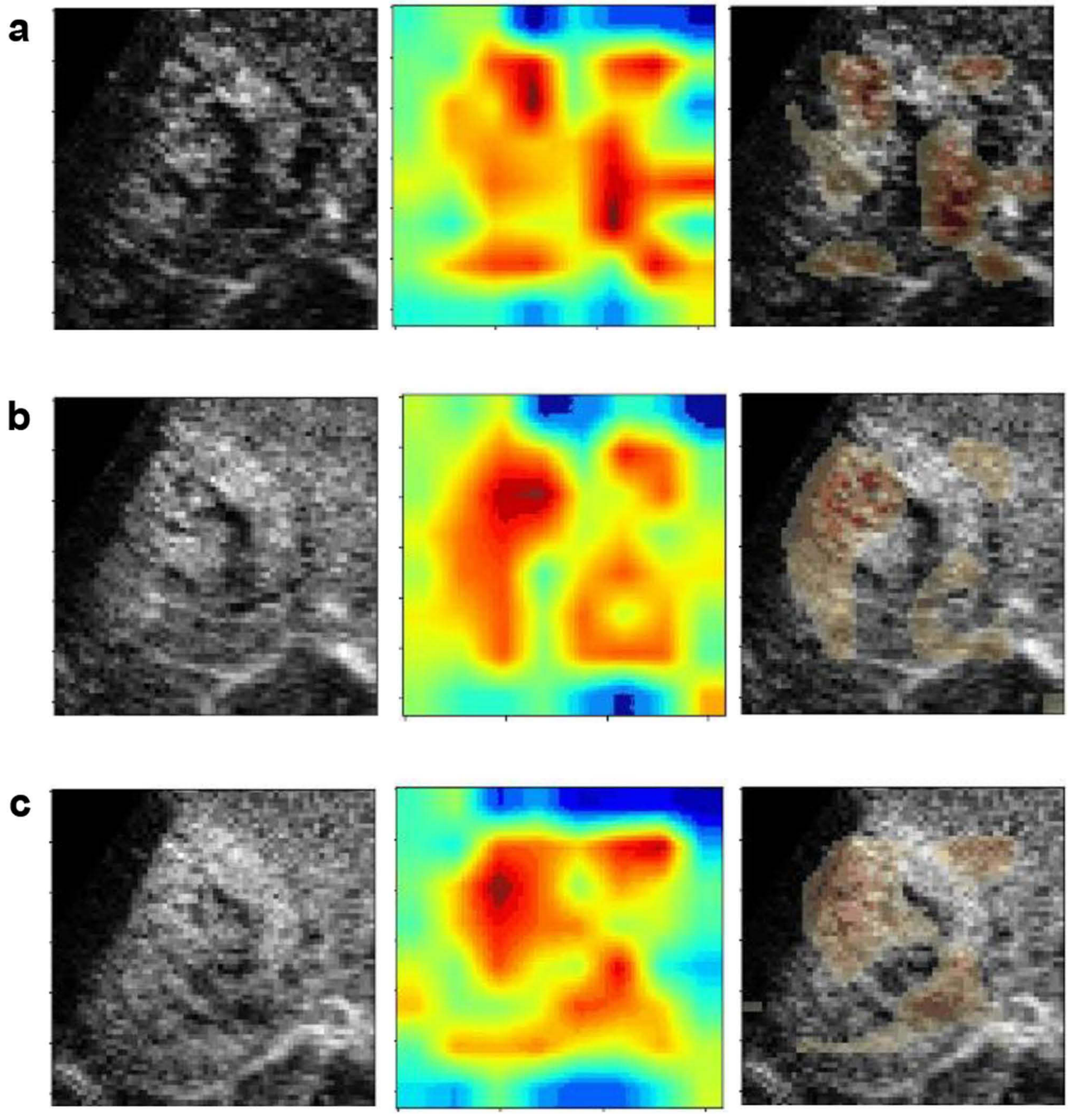

Figure 6 Visualization of the CEUS-LP model. (**a**–**c**) Representative time-point images (9s, 12s, 15s; early period AP) from dynamic CEUS in a post-hepatectomy patient with early recurrence. Each set of images displayed, from left to right, the original monochrome ultrasound image, the pseudo-color heatmap, and the heatmap overlaid on the original ultrasound image.

hypothesize that these heterogeneous attention regions may correspond to areas of necrotic or fibrotic tissue, features often associated with aggressive tumor biology. However, this requires further pathological correlation.

Discussion

This study developed a DL-based model using CEUS to preoperatively predict early recurrence in patients with early-stage HCC patients following hepatectomy. Our results demonstrated that the multiphase CEUS model (CEUS-MP) achieved superior predictive performance compared with single-phase models, with AUC of 0.922 and 0.840 in the training and validation cohorts, respectively. Furthermore, the integration of CEUS-MP signatures with clinical variables (serum albumin and AFP) into a nomogram further enhanced predictive accuracy, yielding AUCs of 0.945 and 0.871 in the training and validation cohorts, respectively. These findings highlighted the potential of CEUS combined with DL as an auxiliary method for preoperative risk stratification in patients with HCC.

While conventional ultrasound remains the first-line imaging tool for liver screening, its inability to assess the tumor vasculature limits its diagnostic and prognostic utility. Since CEUS cines overcome these limitations by providing dynamic, contrast-enhanced visualization of tumor microvasculature, leading to more accurate HCC diagnosis, recurrence prediction, and treatment monitoring.[20] Given these advantages, we utilized CEUS cines, rather than conventional ultrasound images, to develop our prediction models in this study, with the help of advanced quantification techniques for more precise analysis. The superior performance of the CEUS-MP model highlighted the importance of leveraging multiphase CEUS data, which capture dynamic tumor perfusion characteristics across the arterial, portal venous, and late phases. This aligns with previous studies emphasizing the prognostic value of CEUS features, such as rapid wash-in and early wash-out, in HCC recurrence prediction.[12] However, traditional CEUS interpretation is limited by subjectivity and inter-observer variability. Our DL approach addressed this limitation by automatically extracting quantitative features from CEUS cines, thereby standardizing the analysis and improving the reproducibility. Huang et al conducted a quantitative analysis of CEUS images of patients with hepatocellular carcinoma (HCC) following radical resection to predict early recurrence.[21] However, their model achieved an AUC of only 0.57 in the testing cohort, which was significantly lower than that of our proposed model. A potential limitation of their approach was the reliance on a single-frame analysis, the peak contrast intensity of the lesion on CEUS, which may have decreased predictive accuracy. By contrast, our study leveraged continuous multiphase CEUS cine imaging, enabling a more comprehensive assessment and significantly improving the precision of early recurrence prediction.

The integration of CEUS-MP signatures with clinical variables into a nomogram represented a significant advancement in personalized HCC management. Multivariate analysis identified serum albumin and AFP as the independent clinical prognostic predictors. Notably, low ALB levels served as a reliable indicator of advanced hepatic dysfunction, reflecting both the progression of liver carcinogenesis and deteriorating hepatic synthetic capacity.[22] Concurrently, elevated AFP served as a biological marker indicating high invasiveness in HCC.[23] In such patients, some microlesions may escape detection by imaging examinations during the initial HCC diagnosis, contributing to early recurrence after surgical resection. This study demonstrated that higher AFP levels were correlated with an increased risk of early tumor recurrence. Therefore, the AFP level held a significant value in predicting the prognosis of therapy. The high sensitivity and specificity of the nomogram in both cohorts suggested its clinical utility in identifying high-risk patients who may benefit from other treatment selections or intensified surveillance. Notably, the decision curve analysis indicated that the nomogram provided a greater net benefit than the clinical variables alone when the threshold probability exceeded 30%, supporting its practical application in clinical decision-making. The visualization maps further enhanced interpretability, revealing that the model focused on regions with heterogeneous enhancement patterns, which may correlate with aggressive tumor biology. The heterogeneous or peripheral enhancement patterns highlighted by the model were often associated with active tumor regions, while the lack of enhancement in certain areas may correlate with central necrosis or fibrosis commonly found in larger lesions.

Limitations

Our study has several limitations. First, it is a retrospective study conducted at a single center, which introduces potential selection bias. Our patient cohort may not fully represent the more heterogeneous patient populations seen across different healthcare institutions. Second, the uniform high-standard scanning protocols and specialized operators may have inflated the performance estimates of our model. Moreover, the relatively small cohort, particularly the limited number of early recurrence events, is a recognized limitation that warrants caution in interpreting the findings and underscores the need for future validation in larger populations. Furthermore, the use of two different ultrasound systems for CEUS acquisition, despite our efforts at intensity normalization, represents a potential technical confounder. Therefore, the generalizability of our findings needs to be further validated in real-world, multi-center settings, and should also explore incorporating additional imaging modalities (eg, MRI or CT) and molecular biomarkers to refine predictive accuracy.

Conclusion

In conclusion, our study demonstrates that a DL-based CEUS framework, particularly when combined with clinical variables, shows strong potential for the preoperative prediction of early recurrence in patients with HCC undergoing hepatectomy. While these initial results are promising, further validation in large-scale, multi-center, prospective cohorts is essential to confirm its generalizability and establish clinical utility. If validated, this approach could facilitate personalized postoperative management and potentially improve long-term patient outcomes. Future work should also focus on integrating this model with other imaging modalities, such as CT or MRI, to further enhance predictive accuracy.

Ethics Approval and Consent to Participate

This study was approved by the Institutional Review Board of The Second Affiliated Hospital of Nanchang University.

Acknowledgments

The authors thank the data collectors for their efforts and interest in participating in data collection. We would like to thank the patients who willingly provided all the necessary information without any reservation.

Author Contributions

All authors made a significant contribution to the work reported, whether that is in the conception, study design, execution, acquisition of data, analysis and interpretation, or in all these areas; took part in drafting, revising or critically reviewing the article; gave final approval of the version to be published; have agreed on the journal to which the article has been submitted; and agree to be accountable for all aspects of the work.

Funding

This study was supported by grants from the National Natural Science Foundation of China (Grant No. 82360348), the Jiangxi Provincial Natural Science Foundation (Grant No. 20232BAB216096), and the Jiangxi Ganpo Outstanding Talent Support Program–Academic and Technical Discipline Leader Development Project (Grant No. 20243BCE51175).

Disclosure

All authors have no conflicts of interest to declare in this work.

References

1. Forner A, Reig M, Bruix J. Hepatocellular carcinoma. *Lancet*. 2018;391(10127):1301–1314. doi:10.1016/S0140-6736(18)30010-2
2. European Association for the Study of the Liver. EASL clinical practice guidelines: management of hepatocellular carcinoma. *J Hepatol*. 2018;69 (1):182–236. doi:10.1016/j.jhep.2018.03.019
3. Lim KC, Chow PK, Allen JC, et al. Systematic review of outcomes of liver resection for early hepatocellular carcinoma within the Milan criteria. *Br J Surg*. 2012;99:1622–1629. doi:10.1002/bjs.8915

4. Llovet JM, Kelley RK, Villanueva A, et al. Hepatocellular carcinoma. *Nat Rev Dis Primers*. 2021;7(1):6. doi:10.1038/s41572-020-00240-3
5. Poon RT, Fan ST, Ng IO, et al. Different risk factors and prognosis for early and late intrahepatic recurrence after resection of hepatocellular carcinoma. *Cancer*. 2000;89(3):500–507.
6. Villanueva A. Hepatocellular carcinoma. *N Engl J Med*. 2019;380(15):1450–1462. doi:10.1056/NEJMra1713263
7. Lee IC, Huang JY, Chen TC, et al. Evolutionary learning-derived clinical-radiomic models for predicting early recurrence of hepatocellular carcinoma after resection. *Liver Cancer*. 2021;10(6):572–582. doi:10.1159/000518728
8. Kucukkaya AS, Zeevi T, Chai NX, et al. Predicting tumor recurrence on baseline MR imaging in patients with early-stage hepatocellular carcinoma using deep machine learning. *Sci Rep*. 2023;13(1):7579. doi:10.1038/s41598-023-34439-7
9. Yuan C, Wang Z, Gu D, et al. Prediction early recurrence of hepatocellular carcinoma eligible for curative ablation using a Radiomics nomogram. *Cancer Imaging*. 2019;19(1):21. doi:10.1186/s40644-019-0207-7
10. Hui TCH, Chuah TK, Low HM, et al. Predicting early recurrence of hepatocellular carcinoma with texture analysis of preoperative MRI: a radiomics study. *Clin Radiol*. 2018;73(12):1056.e11–1056.e16. doi:10.1016/j.crad.2018.07.109
11. Alzaraa A, Gravante G, Chung WY, et al. Contrast-enhanced ultrasound in the preoperative, intraoperative and postoperative assessment of liver lesions. *Hepatol Res*. 2013;43(8):809–819. doi:10.1111/hepr.12044
12. Cao K, Wu L, Wang X, et al. Risk factors for early recurrence after radical resection of hepatocellular carcinoma based on preoperative contrast-enhanced ultrasound and clinical features. *Technol Cancer Res Treat*. 2024;23:15330338241281327. doi:10.1177/15330338241281327
13. Terzi E, Iavarone M, Pompili M, et al. Contrast ultrasound LI-RADS LR-5 identifies hepatocellular carcinoma in cirrhosis in a multicenter restropective study of 1,006 nodules. *J Hepatol*. 2018;68(3):485–492. doi:10.1016/j.jhep.2017.11.007
14. Wang K, Lu X, Zhou H, et al. Deep learning radiomics of shear wave elastography significantly improved diagnostic performance for assessing liver fibrosis in chronic hepatitis B: a prospective multicenter study. *Gut*. 2019;68(4):729–741. doi:10.1136/gutjnl-2018-316204
15. Ding W, Meng Y, Ma J, et al. Contrast-enhanced ultrasound-based AI model for multi-classification of focal liver lesions. *J Hepatol*. 2025;83(2):426–439. doi:10.1016/j.jhep.2025.01.011
16. Xu W, Zhang H, Zhang R, et al. Deep learning model based on contrast-enhanced ultrasound for predicting vessels encapsulating tumor clusters in hepatocellular carcinoma. *Eur Radiol*. 2025;35(2):989–1000. doi:10.1007/s00330-024-10985-0
17. Hermanek P, Wittekind C. Residual tumor (R) classification and prognosis. *Semin Surg Oncol*. 1994;10(1):12–20. doi:10.1002/ssu.2980100105
18. Yushkevich PA, Piven J, Hazlett HC, et al. User-guided 3D active contour segmentation of anatomical structures: significantly improved efficiency and reliability. *Neuroimage*. 2006;31(3):1116–1128. doi:10.1016/j.neuroimage.2006.01.015
19. Selvaraju RR, Cogswell M, Das A. Grad-CAM: visual explanations from deep networks via gradient-based localization. In: *Proceedings of the IEEE International Conference on Computer Vision*. 2017:618–626.
20. Kudo M, Ueshima K, Osaki Y, et al. B-Mode ultrasonography versus contrast-enhanced ultrasonography for surveillance of hepatocellular carcinoma: a prospective multicenter randomized controlled trial. *Liver Cancer*. 2019;8(4):271–280. doi:10.1159/000501082
21. Huang Z, Shu Z, Zhu RH, et al. Deep learning-based radiomics based on contrast-enhanced ultrasound predicts early recurrence and survival outcome in hepatocellular carcinoma. *World J Gastrointest Oncol*. 2022;14(12):2380–2392. doi:10.4251/wjgo.v14.i12.2380
22. Huang YH, Wu JC, Chen CH, et al. Comparison of recurrence after hepatic resection in patients with hepatitis B vs. hepatitis C-related small hepatocellular carcinoma in hepatitis B virus endemic area. *Liver Int*. 2005;25(2):236–241. doi:10.1111/j.1478-3231.2005.01081.x
23. Yang L, Gu D, Wei J, et al. A radiomics nomogram for preoperative prediction of microvascular invasion in hepatocellular carcinoma. *Liver Cancer*. 2019;8(5):373–386. doi:10.1159/000494099